1-1-1994

Effects Of Spatial Size, Lattice Doubling, And Source Operators On The Hadron Spectrum With Dynamical Staggered Quarks At 6/G(2) = 5.6

Khalil M. Bitar

R. Edwards

U. M. Heller

A. D. Kennedy

Steven Gottlieb

See next page for additional authors

Effects of spatial size, lattice doubling, and source operators on the hadron spectrum with dynamical staggered quarks at $6/g^2=5.6$

Khalil M. Bitar, R. Edwards, U. M. Heller, and A. D. Kennedy
Supercomputer Computations Research Institute, Florida State University, Tallahassee, Florida 32306-4052

Steven Gottlieb
Department of Physics, Indiana University, Bloomington, Indiana 47405

J. B. Kogut
Physics Department, University of Illinois, 1110 West Green Street, Urbana, Illinois 61801

A. Krasnitz
IPS, RZ F3, Eidgenössische Technische Hochschule-Zentrum, CH-8092 Zurich, Switzerland

W. Liu
Thinking Machines Corporation, Cambridge, Massachusetts 02139

Michael C. Ogilvie
Department of Physics, Washington University, St. Louis, Missouri 63130

R. L. Renken
Physics Department, University of Central Florida, Orlando, Florida 32816

D. K. Sinclair
High Energy Physics Division, Argonne National Laboratory, 9700 South Cass Avenue, Argonne, Illinois 60439

R. L. Sugar
Department of Physics, University of California, Santa Barbara, California 93106

D. Toussaint
Department of Physics, University of Arizona, Tucson, Arizona 85721

K. C. Wang
School of Physics, University of New South Wales, Kensington, NSW 2203, Australia
(Received 22 November 1993)

We have extended our previous study of the lattice QCD spectrum with two flavors of staggered dynamical quarks at $6/g^2=5.6$ and $am_q=0.025$ and 0.01 to larger lattices, with better statistics and with additional sources for the propagators. The additional sources allowed us to estimate the Δ mass and to measure the masses of all mesons whose operators are local in time. These mesons show good evidence for flavor symmetry restoration, except for the masses of the Goldstone and non-Goldstone pions. PCAC is observed in that $m_\pi^2 \propto m_q$, and f_π is estimated. Use of undoubled lattices removes the problems with the pion propagator found in our earlier work. Previously we found a large change in the nucleon mass at a quark mass of $am_q=0.01$ when we increased the spatial size from 12 to 16. No such effect is observed at the larger quark mass, $am_q=0.025$. Two kinds of wall source were used, and we have found difficulties in getting consistent results for the nucleon mass between the two sources.

PACS number(s): 12.38.Gc, 11.15.Ha

I. INTRODUCTION

Calculations of hadron spectroscopy remain an important part of nonperturbative studies of QCD using lattice methods. (For reviews of recent progress in this field, see Ref. [1].) We have been engaged in an extended program of calculation of the masses and other parameters of the light hadrons in simulations that include the effects of two flavors of light dynamical quarks. These quarks are realized on the lattice as staggered fermions. We have carried out spectrum calculations with lattice valence quarks in both the staggered and Wilson formulations.

These simulations are performed on $16^3\times 32$ lattices at lattice coupling $\beta=6/g^2=5.6$ with two masses of dynamical staggered fermions, $am_q=0.025$ and $am_q=0.01$. These are the same parameter values as we used in our first round of simulations [2]. However, the first set of simulations had two known inadequacies. The

first was that most of our runs were carried out on lattices of spatial size 12^3. A short run on 16^4 lattices with dynamical quark mass 0.01 showed that the 12^4 lattices were too small: Baryon masses fell by about 15% on the larger lattice compared to the smaller one. Thus it was important to investigate finite-size effects for $am_q=0.025$. We also felt the need for more statistics on the $am_q=0.01$ system for lattices of spatial size 16^3.

Second, nearly all of our earlier running was done on lattices of size 12^4 or 16^4; these lattices were doubled (or quadrupled) in the temporal direction to $12^3\times 24$ (or $12^3\times 48$) or $16^3\times 32$ for spectroscopy studies. Doubling the lattice introduced structure in the propagators of some of the particles: The pion effective mass, in particular, showed peculiar oscillatory behavior as a function of position on the lattice. This behavior was almost certainly due to doubling the lattice [3] and the best way to avoid this problem is to begin with a larger lattice in the temporal direction. Because of these difficulties, mass estimates from such doubled lattices are suspect. This is seen when comparing the masses obtained from the doubled or quadrupled 12^4 lattice with those from the $12^3\times 24$ lattice in our previous work.

In our work on smaller lattices, only one kind of source was used, the so-called "corner" source. In these simulations we include a second kind of source (in fact three sources) which enables us to measure the Δ mass, as well as the nucleon. Furthermore, with these new sources, we are able to measure masses of all mesons created by operators which are local in time and correspond to strictly local continuum operators (local quark bilinears with no derivatives). This allows us to study the extent to which flavor symmetry, which is broken by the staggered lattice, is realized at this lattice spacing.

Some of the results described here have been presented in preliminary form in Ref. [4]. Studies with Wilson valence quarks which complement the results presented here have been published [5] as have studies of Coulomb gauge wave functions [6]. In addition, we are preparing a paper on glueballs and topology. In Sec. II we describe our simulations and in Sec. III we give our results and conclusions.

II. SIMULATIONS

Our simulations were performed on the Connection Machine CM-2 located at the Supercomputer Computations Research Institute at Florida State University.

We carried out simulations with two flavors of dynamical staggered quarks using the hybrid molecular dynamics (HMD) algorithm [7]. The lattice size was $16^3\times 32$ sites, and the lattice coupling $\beta=5.6$. The dynamical quark masses were $am_q=0.01$ and 0.025. A total of 2000 simulation time units (with the normalization of Ref. [2]) was generated at each value of the quark mass, after thermalization. The $am_q=0.01$ run started from an equilibrated 16^4 lattice of our previous runs on the ETA-10, which was doubled in the time direction and then reequilibrated for 150 trajectories. The $am_q=0.025$ run was started from the last configuration of the smaller mass run and then thermalized for 300 trajectories. For $am_q=0.01$ we recorded lattices for the reconstruction of spectroscopy every 5 HMD time units, for a total of 400 lattices. At $am_q=0.025$, lattices were stored every 10 time units for a total of 200 lattices.

For our spectrum calculation, we used periodic boundary conditions in the three spatial directions and antiperiodic boundary conditions in the temporal direction. To calculate hadron propagators, we fixed the gauge in each configuration to the lattice Coulomb gauge using an overrelaxation algorithm [8] and used sources for the quark Green functions which spread out in space uniformly over the spatial simulation volume and were restricted to a single time slice ("wall" sources [9]). Our inversion technique was the conjugate gradient algorithm, using a fast matrix inverter written in CMIS (a low level assembler for the CM-2) by Liu [10,11].

In this work we used two kinds of wall sources. The first of these consisted of a 1 in a selected color component at each site of the source time slice where the x, y, and z coordinates were all odd. In other words, the source was restricted to a single corner of each 2^4 hypercube. This is the same source as used in our previous work, and we will refer to it as the "corner" source or C.

In addition to this corner source, we also used a triplet of wall sources. Following Gupta *et al.* [12] we defined an "even" source which takes the value $+1$ on every site of the source time slice and an "odd" source which is $+1$ on all the even (space odd) sites on the source time slice and -1 on all the odd (space even) sites on this time slice. For definiteness, in this paragraph we take the source time slice to be $t=1$. These sources allowed calculation of the Δ propagator and propagators for some of the local and nonlocal mesons. (We use the Δ propagator corresponding to a point sink where the three quarks are displaced by one unit in the x, y, and z directions, respectively, from the origin of the unit cube [13].) The third source we used was what we call a "vector" source. This source is $+1$ on all sites on the source time slice that have an even y coordinate and -1 for those whose y coordinate is odd. With these three sources we are able to calculate meson propagators for all 20 meson representations of the time slice group which are local in time [14]. In addition, we have calculated the propagator for a local nucleon, and the Δ discussed above, from the "even" source quark Green functions. We will refer to this triplet of sources as EOV.

For the mesons, we averaged propagators computed from six sets of wall sources at time slices 1, 2, 3, 17, 18, and 19. Propagators from three consecutive time slices were needed for a separate study of glueball to $\bar{q}q$ correlations. For the baryons, we used four wall sources at time slices 1, 9, 17, and 25. Propagators from different source slices were averaged together before fitting. (In the case of $m=0.01$ with the corner source, we also fitted the propagators from different sources separately, finding no systematic differences among the different source locations.)

Finally, for comparison, we also measured the hadron propagators from a point source. This calculation was performed "on line" every time unit, for a total of 2000 measurements for each quark mass.

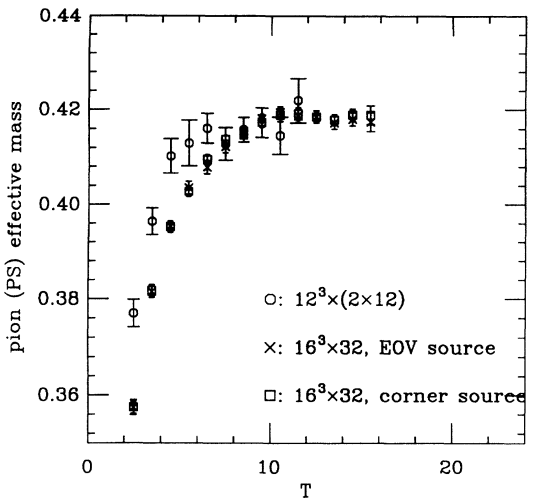

FIG. 1. Pion effective mass vs distance for $am_q = 0.025$.

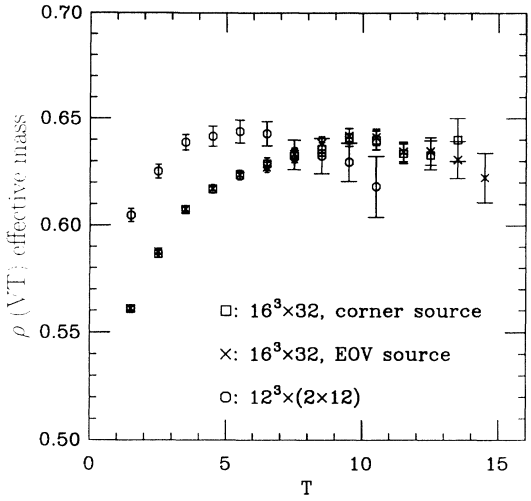

FIG. 3. ρ effective mass vs distance for $am_q = 0.025$.

III. RESULTS

A. Doubling effects on the pion propagator

In our previous, work we used 12^4 and 16^4 lattices doubled or quadrupled in the time direction for computing propagators. We found irregularities in the effective mass as a function of distance from the source for the pion. (The effective mass is the mass obtained by fitting with zero degrees of freedom to points in the propagator centered at some distance.) For the pion propagator, where we fit to a simple exponential plus the piece from periodicity, the effective mass at distance T is obtained from the two points in the propagator at time distances $T-\frac{1}{2}$ and $T+\frac{1}{2}$. For other particles, where we use four parameter fits, with one particle of each parity, the effective masses are obtained from four successive distances in the propagator $(T-\frac{3}{2}, T-\frac{1}{2}, T+\frac{1}{2}, T+\frac{3}{2})$. Since the location of these features seemed to depend on the lattice size before doubling, we tentatively ascribed them to effects of the doubling [2]. A simple analytic model of a doubled lattice showed similar features [3]. In the current work, we generated configurations on a $16^3 \times 32$ lattice, and did not double in the time direction when computing the hadron spectrum. The pion propagator is much better behaved. We show the new results for the pion effective mass together with our previous results in Figs. 1 and 2, for $am_q = 0.025$ and 0.01, respectively. Note that one of the sources used in the present work, the "corner" wall source, is identical to the source used in the previous work. We see that the pion effective mass in the current work is the same for the two sources and is much smoother than on the doubled lattices.

In Figs. 3 and 4 we show the effective mass plots for the ρ. Again, we notice that they are relatively flat, in contrast with the work using doubled lattices [2].

B. Best estimates for masses

Hadron masses were estimated by making correlated fits to the average propagator [15]. To reduce the effects of autocorrelations in simulation time, propagators on several successive lattices were averaged together before

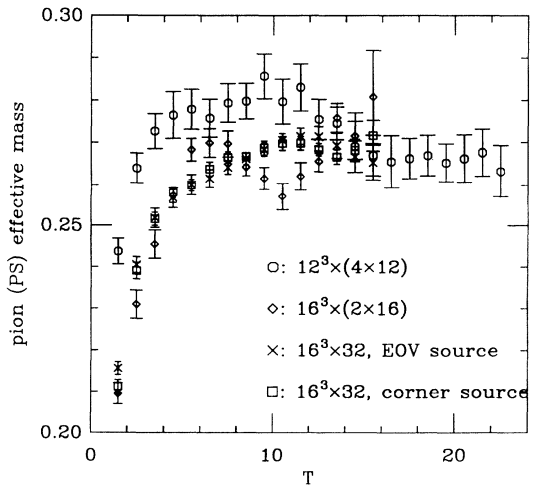

FIG. 2. Pion effective mass vs distance for $am_q = 0.01$.

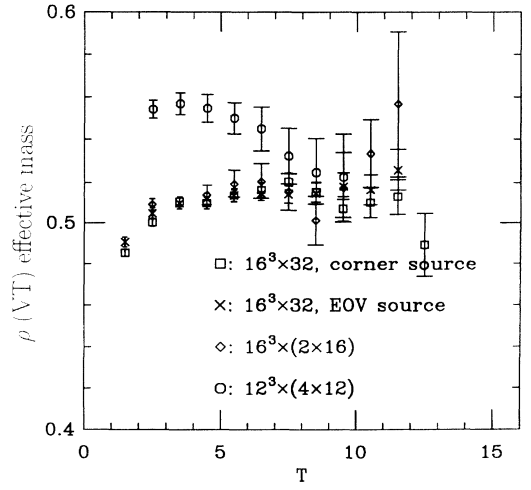

FIG. 4. ρ effective mass vs distance for $am_q = 0.01$.

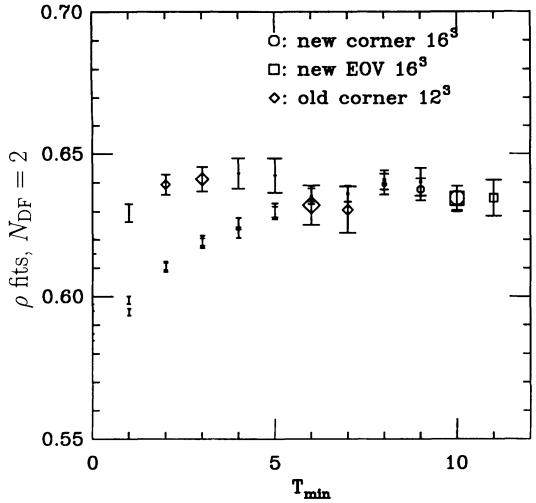

FIG. 5. Fits to the ρ mass for $am_q = 0.025$. The size of the points is proportional to the confidence level of the fits.

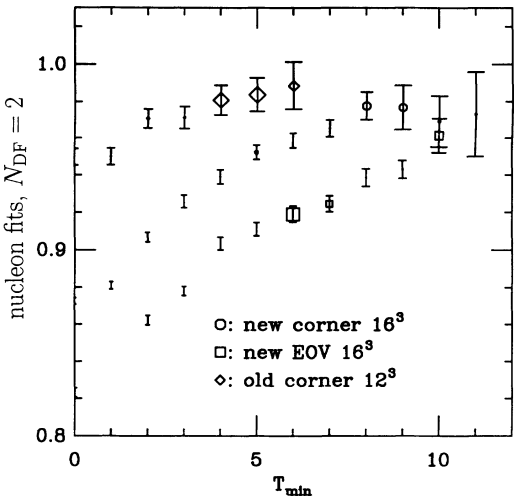

FIG. 7. Fits to the nucleon mass for $am_q = 0.025$. The size of the points is proportional to the confidence level of the fits.

computing the covariance matrix. For example, we most commonly blocked eight lattices together for $am_q = 0.01$ or 40 time units, since we measured every 5 time units. For $am_q = 0.025$ we typically blocked together four lattices, or again 40 time units. These block sizes were chosen based on the observation that increasing the block size to 16 or 8 respectively, did not significantly increase the errors on the masses.

To display the fits we use figures in which the symbol size is proportional to the confidence level of the fits. The symbol size in the keys corresponds to a confidence level of 0.5. We plot the fits as a function of the minimum distance used in the fit. To show how the fit quality varies with distance from the source, we plot the fits with two degrees of freedom. Such fits for the ρ masses are displayed in Figs. 5 and 6 and for the nucleon in Figs. 7 and 8. In Figs. 9 and 10 we show fits for the staggered Δ, for which only even-odd source results on the newer lattices are available.

Tables I–IV give our estimates for the hadron masses. In the continuum, all 15 components of the π multiplet should be degenerate, as should all 15 components of the ρ multiplet. [Although we have only two flavors of quarks in internal lines, the external quark lines have four quark flavors. Hence, in the continuum limit, hadrons form multiplets of flavor SU(4).] When using staggered quarks on the lattice, flavor symmetry is explicitly broken, and each continuum flavor multiplet is broken down into irreducible representations of the discrete symmetries of the lattice action restricted to a given time slice [14]. Full flavor symmetry should be restored in the continuum limit. The extent to which this symmetry is restored at a finite lattice spacing gives us some indication as to whether our lattice spacing is small enough (β large enough) to adequately approximate the continuum limit. In Figs. 11 and 12 we plot the π and ρ masses, re-

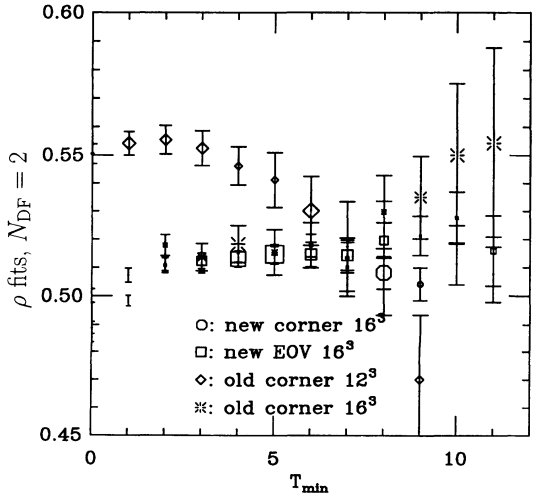

FIG. 6. Fits to the ρ mass for $am_q = 0.01$. The size of the points is proportional to the confidence level of the fits.

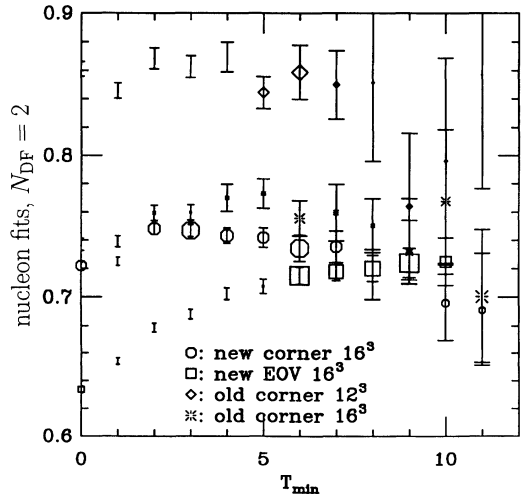

FIG. 8. Fits to the nucleon mass for $am_q = 0.01$. The size of the points is proportional to the confidence level of the fits.

spectively, from Tables I–IV for the different representations of the time slice group accessible using the EOV sources. We notice that flavor symmetry appears to be good to a few percent for the ρ multiplet. For the π sector there is approximate degeneracy for the non-Goldstone pions, but the mass of the Goldstone pion still lies significantly below that of the rest [$(m_{\tilde{\pi}}-m_{\pi})/m_{\pi}\approx 0.3$ for $am_q=0.01$]. This should not surprise us since, for the quenched approximation, definitive evidence for the restoration of the mass degeneracy between the Goldstone and non-Goldstone pions has only been claimed for $\beta=6.5$ [16]. In Sec. III E we shall indicate that our β [Eq. (5.6)] is more comparable with a quenched system at $\beta\approx 5.95$. The squared Goldstone pion mass is very nearly proportional to m_q (see Sec. III D). The other pion masses do not extrapolate to zero with m_q. For example, at $am_q=0.025$ the mass ratio $m_{\tilde{\pi}}/m_{\pi}=1.223(5)$, while at $am_q=0.01$ this ratio is 1.306(11). This contrasts with a four flavor study by the MT_c Collaboration [17], in which $m_{\tilde{\pi}}^2$ appears to be proportional to m_q.

Figure 13 gives the "Edinburgh" plot of m_N/m_{ρ} against m_{π}/m_{ρ} for the results of Tables I–IV. Figure 14 is the "Boulder" plot for the N-Δ mass splitting. Both

TABLE I. Hadron masses at $am_q=0.01$. Notation: the superscript is the dimension of the representation of the time slice group; the number of links is in parentheses; the tilde state has an extra γ_0; the notation is abbreviated when unambiguous. "NP" indicates no plateau was found in the mass fits.

			$am_q=0.01$				
Particle	Source	Range	Mass	Error	$\chi^2/N_{\rm DF}$	Confidence	Parameters
π	Point	12–16	0.2681	0.0010	0.13	0.95	2
π	EOV	7–16	0.2667	0.0008	1.90	0.55	2
π	EOV	1–16	0.2673	0.0008	1.50	0.12	4
π	C	13–16	0.2667	0.0015	1.45	0.24	2
π	C	4–16	0.2700	0.0012	1.33	0.20	4
$\tilde{\pi}$	Point	9–16	0.3899	0.0190	1.27	0.28	4
$\tilde{\pi}$	EOV	6–16	0.3500	0.0026	0.885	0.52	4
$\tilde{\pi}$	C	9–16	0.3553	0.0039	0.20	0.94	4
$\pi^3(1)$	EOV	5–16	0.3474	0.0014	1.99	0.30	2
$\tilde{\pi}^3(1)$	EOV	6–16	0.3694	0.0032	0.77	0.61	4
$\pi^3(2)$	EOV	7–16	0.3703	0.0019	1.25	0.19	2
$\tilde{\pi}^3(2)$	EOV	8–16	0.3842	0.0034	1.30	0.26	4
$\pi(3)$	EOV	7–16	0.3831	0.0021	0.89	0.52	2
η'/π	EOV	6–16	0.3952	0.0036	0.44	0.88	4
ρ	Point	9–16	0.492	0.038	0.65	0.63	4
ρ	EOV	3–16	0.5133	0.0022	1.11	0.35	4
ρ	C	8–16	0.5085	0.0050	1.54	0.17	4
$\tilde{\rho}$	Point	8–16	0.476	0.035	0.31	0.91	4
$\tilde{\rho}$	EOV	4–16	0.5152	0.0032	1.74	0.07	4
$\tilde{\rho}$	C	10–16	0.4918	0.0091	0.40	0.74	4
ω/ρ	EOV	2–16	0.5206	0.0025	1.31	0.21	4
$\tilde{\rho}^3(1)$	EOV	2–16	0.5184	0.0030	0.85	0.59	4
$\rho^6(1)$	EOV	4–16	0.5207	0.0025	0.64	0.76	4
$\tilde{\rho}^6(1)$	EOV	3–16	0.5205	0.0024	1.13	0.34	4
$\rho^3(2)$	EOV	5–16	0.5173	0.0035	1.05	0.39	4
$\tilde{\rho}^3(2)$	EOV	2–16	0.5180	0.0032	0.92	0.52	4
$\rho^6(2)$	EOV	3–16	0.5221	0.0019	0.88	0.55	4
$\tilde{\rho}^6(2)$	EOV	5–16	0.5134	0.0038	1.29	0.24	4
$\rho(3)$	EOV	2–16	0.5229	0.0022	0.75	0.69	4
$\tilde{\rho}(3)$	EOV	3–16	0.5186	0.0031	0.73	0.70	4
N	Point	9–14	0.738	0.086	0.47	0.63	4
N	EOV	7–15	0.720	0.006	0.36	0.88	4
N	C	10–15	0.696	0.027	2.00	0.37	4
N	C	0–15	0.727	0.008	0.31	0.96	8
N'	Point	NP	NP	NP	NP	NP	4
N'	Point	7–13	1.209	0.087	1.21	0.30	4
N'	EOV	6–15	0.948	0.066	0.37	0.90	4
N'	EOV	0–15	0.948	0.025	0.31	0.96	8
N'	C	3–15	0.904	0.009	1.78	0.06	4
Δ	EOV	4–15	0.850	0.008	0.39	0.93	4
Δ'	EOV	6–15	1.031	0.065	0.47	0.83	4

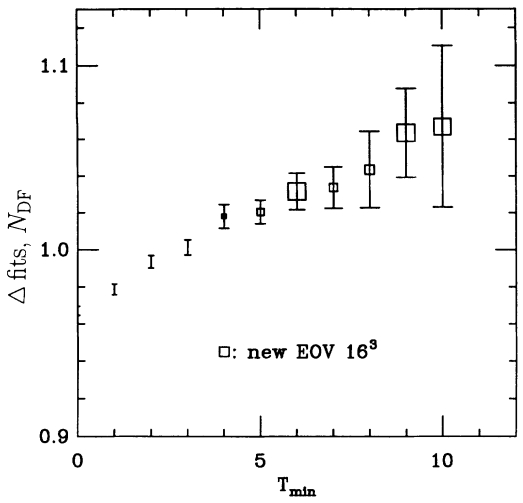

FIG. 9. Fits to the Δ mass for $am_q=0.025$. The size of the points is proportional to the confidence level of the fits.

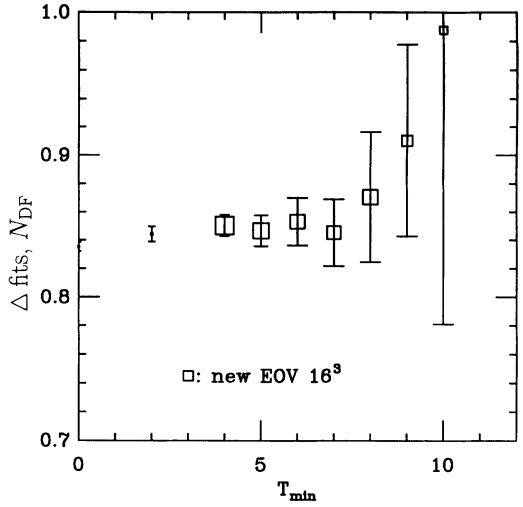

FIG. 10. Fits to the Δ mass for $am_q=0.01$. The size of the points is proportional to the confidence level of the fits.

plots are roughly what one would expect for these values of the quark mass.

C. Finite-size and source effects on the hadron masses

In our earlier work we found a large change in the nucleon mass with quark mass $am_q=0.01$ when the spatial lattice size was increased from 12 to 16. With our new results we can examine this in more detail, as well as extend the study to $am_q=0.025$.

For $am_q=0.01$, the nucleon mass on a $12^3\times(12\times2)$ lattice was estimated to be 0.848(11) while that on a $12^3\times24$ was found to be 0.815(13), the difference probably being an effect of the doubling. On the $16^3\times(16\times2)$, this had fallen to 0.770(8). In the data of Table I for the $16^3\times32$ lattice, we find that for the "corner" source

TABLE II. Hadron masses at $am_q=0.01$. The notation is the same as in Table I. The "?" denotes cases where none of the fits were good. The π^* is an excited state in the pion channel.

			$am_q=0.01$				
Particle	Source	Range	Mass	Error	χ^2/N_{DF}	Confidence	Parameters
π^*	EOV	1–16	0.893	0.021	1.50	0.12	4
π^*	C	4–16	0.578	0.063	1.33	0.20	4
π^*	Point	5–16	0.789	0.033	1.87	0.06	4
f_0/a_0	Point	10–16	0.547	0.015	1.61	0.19	4
f_0/a_0	EOV	6–16	0.514	0.008	0.89	0.52	4
f_0/a_0	C	7–16	0.505	0.013	0.78	0.59	4
$a_0^3(1)$	EOV	6–16	0.615	0.014	0.77	0.61	4
$a_0^3(2)$	EOV	6–16	0.615	0.019	1.53	0.15	4
$a_0(3)$	EOV	6–16	0.645	0.020	0.44	0.88	4
a_1	Point	8–16	0.683	0.097	0.31	0.91	4
a_1	EOV	5–16	0.700	0.011	1.88	0.06	4
a_1	C	6–16	0.744(?)	0.020	2.71	0.008	4
$a_1^3(1)$	EOV	3–16	0.693	0.007	0.93	0.51	4
$a_1^6(1)$	EOV	6–16	0.712	0.013	1.18	0.31	4
$a_1^3(2)$	EOV	5–16	0.655	0.018	0.57	0.80	4
$a_1^6(2)$	EOV	3–16	0.701	0.004	1.27	0.24	4
$a_1(3)$	EOV	4–16	0.726	0.011	0.80	0.62	4
b_1	Point	7–16	0.818	0.135	0.95	0.46	4
b_1	EOV	3–16	0.686	0.008	1.11	0.35	4
b_1	C	6–16	0.775(?)	0.042	1.86	0.08	4
$b_1^3(1)$	EOV	2–16	0.719	0.007	1.31	0.21	4
$b_1^6(1)$	EOV	5–16	0.739	0.015	0.63	0.76	4
h_1/b_1	EOV	5–16	0.732	0.019	1.05	0.39	4
$b_1^6(2)$	EOV	2–16	0.717	0.004	1.05	0.40	4
$b_1(3)$	EOV	2–16	0.711	0.006	0.75	0.69	4

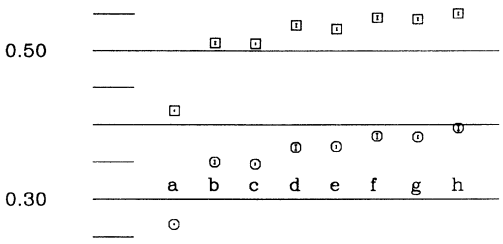

FIG. 11. Masses of the various lattice pions. The octagons are for $am_q=0.01$ and the squares for $am_q=0.025$. From left to right, the representations are (a) π (Goldstone), (b) $\tilde{\pi}$, (c) $\pi^3(1)$, (d) $\tilde{\pi}^3(1)$, (e) $\pi^3(2)$, (f) $\tilde{\pi}^3(2)$, (g) $\pi(3)$, and (h) the η'/π.

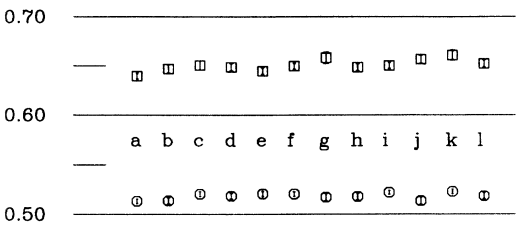

FIG. 12. Masses of the various lattice ρ mesons. From left to right the representations are (a) ρ (VT), (b) $\tilde{\rho}$ (PV), (c) ω/ρ, (d) $\tilde{\rho}^3(1)$, (e) $\rho^6(1)$, (f) $\tilde{\rho}^6(1)$, (g) $\rho^3(2)$, (h) $\tilde{\rho}^3(2)$, (i) $\rho^6(2)$, (j) $\tilde{\rho}^6(2)$, (k) $\rho(3)$, and (l) $\tilde{\rho}(3)$.

TABLE III. Hadron masses at $am_q=0.025$. The notation is the same as in Table I.

			$am_q=0.025$				
Particle	Source	Range	Mass	Error	χ^2/N_{DF}	Confidence	Parameters
π	Point	13–16	0.4188	0.0005	1.67	0.17	2
π	Point	4–16	0.4190	0.0005	1.68	0.09	4
π	EOV	10–16	0.4185	0.0009	0.90	0.48	2
π	EOV	1–16	0.4193	0.0007	1.13	0.33	4
π	C	9–16	0.4185	0.0006	0.63	0.70	2
π	C	1–16	0.4192	0.0006	0.45	0.94	4
$\tilde{\pi}$	Point	9–16	0.5120	0.0061	1.43	0.22	4
$\tilde{\pi}$	EOV	8–16	0.5106	0.0018	1.05	0.39	4
$\tilde{\pi}$	C	10–16	0.5089	0.0027	0.63	0.59	4
$\pi^3(1)$	EOV	9–16	0.5098	0.0012	0.72	0.64	2
$\tilde{\pi}^3(1)$	EOV	8–16	0.5347	0.0025	1.20	0.30	4
$\pi^3(2)$	EOV	9–16	0.5297	0.0017	0.42	0.87	2
$\tilde{\pi}^3(2)$	EOV	9–16	0.5451	0.0028	0.96	0.43	4
$\pi(3)$	EOV	9–16	0.5431	0.0018	0.69	0.66	2
η'/π	EOV	6–16	0.5507	0.0020	0.53	0.82	4
ρ	Point	10–16	0.6243	0.0127	0.40	0.75	4
ρ	EOV	7–16	0.6396	0.0028	1.33	0.24	4
ρ	C	8–16	0.6396	0.0037	1.00	0.42	4
$\tilde{\rho}$	Point	NP	NP	NP	NP	NP	4
$\tilde{\rho}$	EOV	8–16	0.6471	0.0043	0.77	0.57	4
$\tilde{\rho}$	C	6–16	0.6437	0.0037	0.60	0.76	4
ω/ρ	EOV	8–16	0.6507	0.0047	0.45	0.81	4
$\tilde{\rho}^3(1)$	EOV	6–16	0.6489	0.0038	1.98	0.05	4
$\rho^6(1)$	EOV	8–16	0.6449	0.0031	0.92	0.47	4
$\tilde{\rho}^6(1)$	EOV	7–16	0.6498	0.0029	0.64	0.70	4
$\rho^3(2)$	EOV	9–16	0.6584	0.0057	1.28	0.28	4
$\tilde{\rho}^3(2)$	EOV	6–16	0.6488	0.0036	0.58	0.77	4
$\rho^6(2)$	EOV	8–16	0.6505	0.0029	0.48	0.79	4
$\tilde{\rho}^6(2)$	EOV	8–16	0.6568	0.0041	0.77	0.57	4
$\rho(3)$	EOV	9–16	0.6610	0.0051	1.24	0.29	4
$\tilde{\rho}(3)$	EOV	7–16	0.6524	0.0035	2.95	0.07	4
N	Point	10–15	0.926	0.028	0.17	0.84	4
N	EOV	2–15	0.949	0.010	1.83	0.10	8
N	C	8–15	0.979	0.008	1.40	0.23	4
N'	Point	NP	NP	NP	NP	NP	4
N'	EOV	2–15	1.289	0.078	1.83	0.10	8
N'	C	8–15	1.137	0.089	1.40	0.23	4
Δ	EOV	6–15	1.035	0.010	0.33	0.92	4
Δ'	EOV	6–15	1.302	0.070	0.33	0.92	4

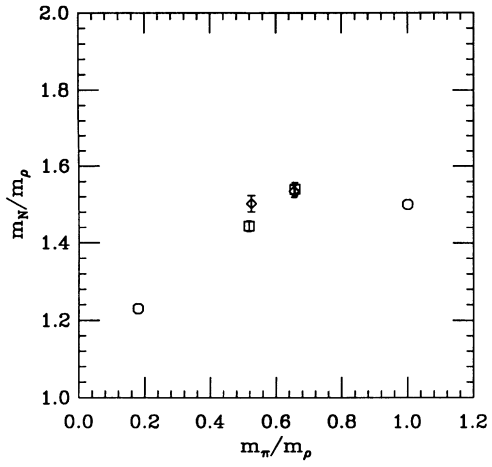

FIG. 13. Edinburgh plot. The diamonds are our results from the previous simulations, and the squares are the new results. Error bars are the statistical errors only and do not include uncertainty based on the choice of source or fitting range. (We use the even-odd source results here.)

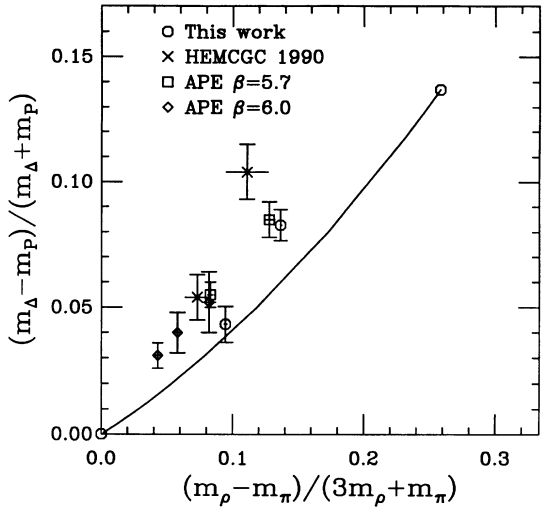

FIG. 14. Comparison of baryon and meson hyperfine splitting. The two circles show the expected values of hyperfine splitting in the limit of infinite quark mass and from experiment; the line interpolating between them is a simple quark model. The APE data is from a quenched simulation [18].

(which is identical to the source used on the smaller lattices) the value is 0.748(4) again lower than the doubled case. Thus we have further evidence for the finite volume effect reported in [2] and also seen by [19] for the nucleon mass. At $am_q=0.025$, the nucleon mass on a $12^3\times(12\times2)$ lattice was 0.982(9), while that for a $16^3\times32$ lattice (Table III) is 0.981(8). Thus it would appear that even a 12^3 box is adequate to hold a nucleon at $am_q=0.025$ with no appreciable finite-size effects.

For the mesons we find good agreement between the masses on $12^3\times24$, $16^3\times(16\times2)$, and the new results on $16^3\times32$ lattices for both quark masses. The $12^3\times(12\times2)$ ρ effective masses showed no clear plateau, and this is

TABLE IV. Hadron masses at $am_q=0.025$. The notation is the same as in Table I.

			$am_q=0.025$				
Particle	Source	Range	Mass	Error	χ^2/N_{DF}	Confidence	Parameters
π^*	Point	7–16	0.845	0.072	1.41	0.21	4
π^*	EOV	1–16	0.842	0.012	1.13	0.33	4
π^*	C	1–16	0.853	0.006	0.45	0.94	4
f_0/a_0	Point	9–16	0.696	0.007	1.43	0.22	4
f_0/a_0	EOV	8–16	0.699	0.010	1.05	0.39	4
f_0/a_0	C	8–16	0.697	0.015	1.40	0.23	4
$a_0(1)$	EOV	8–16	0.848	0.030	1.20	0.30	4
$a_0(2)$	EOV	6–16	0.827	0.018	1.36	0.22	4
$a_0(3)$	EOV	6–16	0.829	0.020	0.53	0.82	4
a_1	Point	NP	NP	NP	NP	NP	4
a_1	EOV	6–16	0.886	0.022	1.38	0.21	4
a_1	C	6–16	0.892	0.021	0.60	0.76	4
$a_1^3(1)$	EOV	7–16	0.887	0.036	1.74	0.11	4
$a_1^6(1)$	EOV	6–16	0.905	0.018	0.93	0.48	4
$a_1^3(2)$	EOV	6–16	1.023	0.040	0.58	0.77	4
$a_1^6(2)$	EOV	8–16	0.927	0.044	0.77	0.57	4
$a_1(3)$	EOV	NP	NP	NP	NP	NP	4
b_1	Point	NP	NP	NP	NP	NP	4
b_1	EOV	7–16	0.823	0.067	1.33	0.24	4
b_1	C	8–16	1.011	0.096	1.00	0.42	4
$b_1^3(1)$	EOV	6–16	0.973	0.044	0.99	0.43	4
$b_1^6(1)$	EOV	7–16	0.843	0.026	0.95	0.46	4
h_1/b_1	EOV	7–16	0.814	0.050	1.72	0.11	4
$b_1^6(2)$	EOV	7–16	0.855	0.032	0.65	0.69	4
$b_1(3)$	EOV	7–16	0.873	0.063	1.96	0.07	4

reflected in the other fits, so that the mass values were unreliable. The observed undulating behavior of the π effective masses on the $12^3\times(12\times2)$ lattice reflects itself in the more general fit. [The $16^3\times(16\times2)$ lattice shows similar problems.] Within these ambiguities, the new results are in good agreement with those for smaller lattices. Hence we may conclude that there are no significant finite-size effects in the meson masses for spatial boxes with volumes $\gtrsim 12^3$ for quark masses $am_q \gtrsim 0.01$ at $\beta=5.6$.

In an effort to compare finite-size effects seen in different simulations with two quark flavors, we plot the results of several groups in Figs. 15 and 16. We show the ρ and nucleon mass at each size normalized by its infinite-volume limit as a function of the linear size of the box. For the simulations with $6/g^2=5.6$ and 5.7, where the maximum size is not that large, we calculate the infinite-volume limit by fitting the finite-size data assuming the finite-size effect falls as $1/V$. For the $6/g^2=5.47$ results, we just use the largest volume. To determine the box size, we must know the lattice spacing in fm. We have chosen to determine the lattice spacing simply by setting the ρ mass to 770 MeV. We know that at these quark masses, the ρ is heavier than 770 MeV, but if the different simulations have similar π to ρ mass ratios, then the error from our assumption should be similar in each case. For our simulations, $m_\pi/m_\rho=0.66$ and 0.52 for $am_q=0.025$ and 0.01, respectively. For the simulations at $6/g^2=5.7$, $am_q=0.01$ and $m_\pi/m_\rho=0.59$. For the simulations at 5.47, the mass ratio is 0.60. If one were to correct for the fact that our mass ratios are not exactly what is seen in the other simulations, the $am_q=0.025$ points in Figs. 15 and 16 would shift to the left and the 0.01 mass points would shift to the right. We see that for mass 0.01 the results here are comparable to what has been seen in other calculations. For the heavier quark mass, the effects seem to be somewhat smaller.

Now let us discuss the effects of the two different types of source. For mesons, there is only one wall source and one point sink corresponding to each component of each irreducible representation of the time slice group [14]. This means that for those representations occurring in both the "corner" and EOV wall sources we can expect to get the same results in both cases. This is well borne out by the masses of Tables I–IV.

For the nucleon we use a local sink which projects the **8** representation of the time slice group. The "corner" source produces only one baryon representation, the local **8** representation. The "even" source, on the other hand, produces all baryon representations, and in particular five copies of the **8** representation. Only one of these **8**'s is local; the other four have quarks on more than one vertex of the unit cube. The local point sink has overlap with all five of these octets, each of which will, in general, have different couplings to the allowed baryon states. For this reason the nucleon propagator for the "even" source can be rather different from that for the corner source. That this is so is illustrated by looking at the effective mass plots (Figs. 17 and 18) for the two different nucleon propagators. At $am_q=0.025$, the effective masses for the "corner" source lie consistently higher than those for the "even" source. Since it is difficult to find strong evidence for a plateau in these data (at least not for the "corner source"), the problem could well be that the plateau starts just as the signal/noise ratio starts to worsen. In any case, our best fits (Table III) are within two standard deviations of one another and can thus be considered to be consistent. For $am_q=0.01$, the effective masses for the "corner" nucleon again lie consistently above those for the "even" source. However, in the graph of Fig. 18, one notes that the effective masses for the two sources appear to be coming together for $T\gtrsim 7.5$. If this is correct, the reason for the discrepancy between the two estimates of the nucleon mass is that our fitting criterion favors the false plateau $3.5\lesssim T\lesssim 6.5$ in the nucleon effective mass

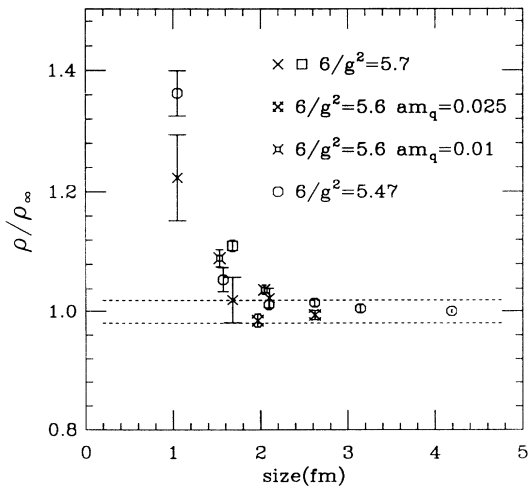

FIG. 15. ρ mass normalized by its infinite-volume limit plotted as a function of physical lattice size. The determination of the lattice spacing is discussed in the text. Results for $6/g^2=5.7$ are taken from Refs. [19,20]. Results for 5.47 are from Ref. [21].

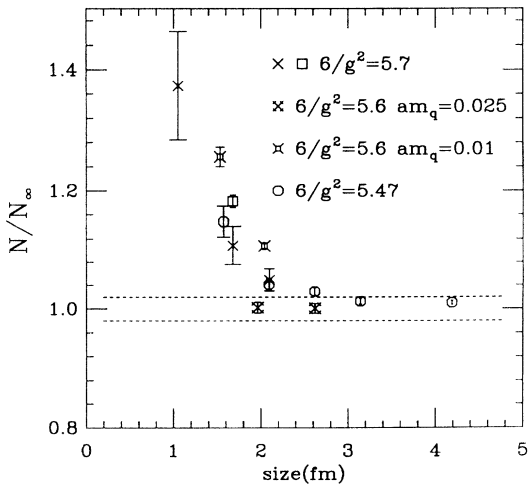

FIG. 16. Nucleon mass normalized by its infinite-volume limit plotted as a function of lattice size. The notation and sources of data are the same as in Fig. 15.

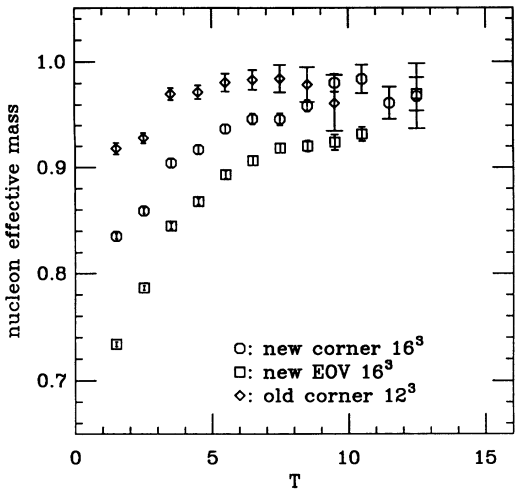

FIG. 17. Nucleon effective mass vs distance for $am_q=0.025$.

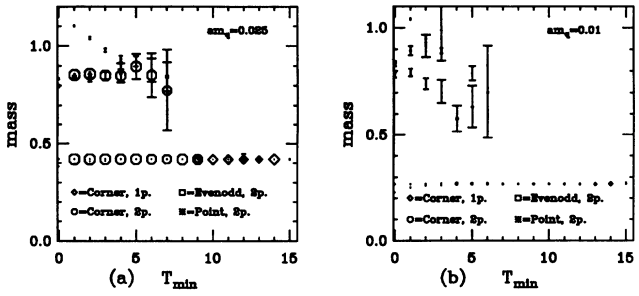

FIG. 19. Goldstone pion fits including excited state masses. The symbol size is proportional to the confidence level, with the symbol size used in the legend corresponding to 50% confidence. We show results for $am_q=0.025$ (a) and 0.01 (b). The octagons, squares, and bursts correspond to two-particle fits, both particles having the same parity, with corner, EOV, and point sources, respectively, while the diamonds are from one-particle fits to the corner wall source.

plot. If we had better statistics, we would presumably find the true plateau.

Finally, let us comment on the point source fits as compared with the wall fits. Only in the case of the π do these point source fits have the quality of the wall fits. The π masses obtained from the point and wall sources are in excellent agreement. For the other particles, the rapid decrease of the point source propagators with increasing T due to contamination with higher-mass excitations produces mass estimates that tend to be high and at the very least have much larger errors than the wall results. The rapid decrease of effective masses with T for the point sources makes the evidence that these reach a plateau before the signal is lost less compelling than in the case of wall sources. Their main virtue is that their mass predictions give an upper bound on the particle mass. This is no great advantage if the bound is too large or has a very large uncertainty (error).

For the opposite-parity vector mesons a_1 and b_1, the results are not nearly as good. In Tables II and IV, we see that the different representations have much larger scatter than for the ρ mass estimates and that the statistical errors are much larger. In general, the masses for these particles are smaller than experiment, being lower than the nucleon mass. There is some evidence that this situation is improving as the quark mass is lowered, but the large errors on these masses at $am_q=0.025$ make it impossible to make firm statements.

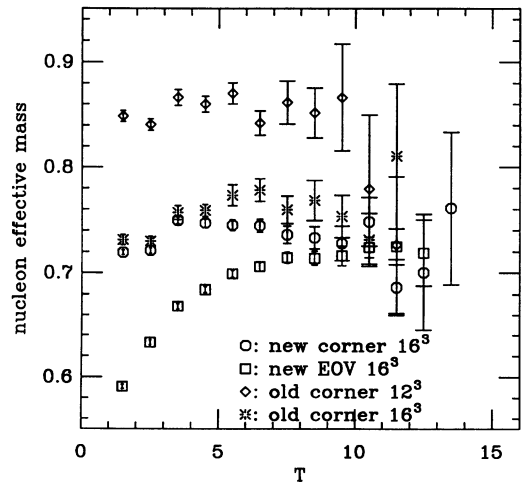

FIG. 18. Nucleon effective mass vs distance for $am_q=0.01$.

Eventually, lattice QCD should provide masses for excited state hadrons as well as for the lowest-mass particle for given quantum numbers. Identification of excited states is probably easiest in the pion channel, since the small ground-state mass means that the excited state is probably well separated in mass from the ground state. In Fig. 19 we show fits to the pion from Euclidean time range $T_{\min}$ to 16, including both the ground- and excited-state masses for the two particle fits (both with the same parity). In these graphs the symbol size is proportional to the confidence level of the fits. At $am_q=0.025$, we see consistent results for the excited state mass, independent of $T_{\min}$ up to the point where the excited state is no longer needed in the fit and independent of whether we use the EOV or the corner wall source. For the point source, we see that including two particles is still not sufficient to get good fits with small $T_{\min}$. Unfortunately, for $am_q=0.01$ the results are not nearly as good, although this is one of the cases for which we have no good fits even with large $T_{\min}$.

D. Lattice spacing and PCAC

The lattice spacing a can be estimated from any dimensional quantity for which an experimental number is known. Since at current lattice spacings the ratios of masses calculated on the lattice do not quite match experiment, the result will depend on which quantity is chosen as the standard. If we use the ρ mass linearly extrapolated to $m_q=0$, we find $a^{-1}=1.80(2)$ GeV (from the EOV ρ). Similarly, if we linearly extrapolate the nucleon mass, we find $a^{-1}=1.65(6)$ GeV. We have also measured hadrons using Wilson valence quarks on these lattices [22]. If we extrapolate the valence quark κ to κ_c and the

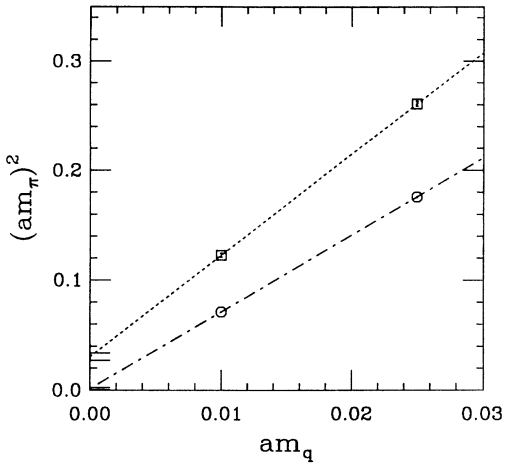

FIG. 20. Squared pion masses vs quark mass. The octagons are for the Goldstone pion, and the squares for the other point-like pion, the $\tilde{\pi}$. The dashed and dotted lines are extrapolations to zero quark mass, and the horizontal lines on the left side are one standard deviation limits on this extrapolation. (In reality, we do not expect the $\tilde{\pi}$ mass squared to be vanish linearly with m_q for small m_q.)

dynamical quark mass to zero, we find lattice spacings of $a^{-1}=2.24(9)$ and 1.87(12) from the valence Wilson ρ and nucleon, respectively. In a separate work, a lattice spacing was estimated from the heavy quark potential on these lattices, with the result that $a^{-1}=2.14(16)$ GeV [23].

PCAC (partial conservation of axial vector current) predicts that $m_\pi^2 \propto m_q$. In Fig. 20 we plot m_π^2 against m_q. For definiteness we have chosen the four-parameter EOV estimate for the pion mass in each case. We obtain

$$m_\pi^2 = 0.0013(9) + 6.98(5) m_q \ .$$

The intercept is only 1.4σ from zero. Thus this simple PCAC relationship appears to be well satisfied. We therefore can make use of the more precise relationship

$$f_\pi^2 m_\pi^2 = m_q \langle \bar{\psi}\psi \rangle \ ,$$

for m_q sufficiently small, to extract an estimate for f_π. To finesse the question of perturbative subtractions for $\langle \bar{\psi}\psi \rangle$ which are known to remove most of its apparent mass dependence, we linearly extrapolate it to $m_q=0$ where no such subtraction is necessary. Our measured values for $a^3\langle \bar{\psi}\psi \rangle$ were 0.112 23(46) at $am_q=0.01$ and 0.213 98(34) for $am_q=0.025$. This gives $a^3\langle \bar{\psi}\psi \rangle = 0.044\,40(80)$ at $m_q=0$. Since $\langle \bar{\psi}\psi \rangle$ is measured with four fermion flavors, we must multiply it by $(N_f=2)/4=0.5$ before inserting it into the above equation, giving

$$af_\pi = 0.0564(5) \ .$$

Using a estimated from extrapolating the ρ mass, we find

$$f_\pi = 102(2) \text{ MeV} \ ,$$

as compared with the experimental value $f_\pi \approx 93$ MeV. Note that the error we have quoted represents only the statistical error. Just taking into account the systematic uncertainty of choosing which ρ mass to use indicates that the error estimate should almost certainly be at least twice what we have quoted. With this in mind and remembering that we really have little justification for linearly extrapolating our ρ masses to $m_q=0$, we consider this value to be quite good.

E. Comparison between quenched and full QCD

In addition to simulating with two flavors of dynamical quarks, we also estimated the hadron spectrum for quenched QCD on a $16^3 \times 32$ lattice. Here the aim was to compare the spectrum from quenched QCD with that of full QCD. For this reason, we chose β values for the quenched runs which we believed to be in close correspondence with $\beta=5.6$ for full (two flavor) QCD. Two values of β were chosen so that interpolation to a requisite β might be possible. We chose $\beta=5.85$ and 5.95 as our two values. The hadron masses for these β's at $am_q=0.01$ and $am_q=0.025$ are given in Tables V and VI. A cursory comparison of the masses in these tables with those for the full theory (Tables I–IV) shows why these two β values were chosen. At $\beta=5.85$ the masses (in lattice units) of the Goldstone pions are very close to their values in the full theory for both quark masses. At $\beta=5.95$, on the other hand, the masses of the ρ and nucleon at $am_q=0.01$ are close to the values in full QCD.

TABLE V. Quenched hadron masses at $\beta=5.85$.

$\beta=5.85$							
	$am_q=0.01$				$am_q=0.025$		
Particle	Range	Mass	Error	Particle	Range	Mass	Error
π	7–14	0.2743	0.0005	π	9–14	0.4243	0.0008
$\tilde{\pi}$	7–15	0.4385	0.0080	$\tilde{\pi}$	6–14	0.5577	0.0048
ρ	6–14	0.6476	0.0149	ρ	6–13	0.7183	0.0056
$\tilde{\rho}$	4–14	0.6258	0.0084	$\tilde{\rho}$	4–12	0.7126	0.0040
f_0/a_0	5–13	0.5624	0.0321	f_0/a_0	6–14	0.8075	0.0314
a_1	2–9	0.8323	0.0179	a_1	4–12	0.9832	0.0284
b_1	6–14	1.553	0.539	b_1	6–13	1.274	0.213
N	5–13	0.9501	0.0276	N	5–13	1.060	0.008
N'	5–13	0.7290	0.0981	N'	5–13	1.184	0.065

TABLE VI. Quenched hadron masses at $\beta=5.95$.

$\beta=5.95$							
	$am_q=0.01$				$am_q=0.025$		
Particle	Range	Mass	Error	Particle	Range	Mass	Error
π	6–14	0.2501	0.0009	π	6–14	0.3875	0.0007
$\tilde{\pi}$	8–16	0.3215	0.0044	$\tilde{\pi}$	4–12	0.4512	0.0020
ρ	3–11	0.5159	0.0040	ρ	6–14	0.5954	0.0028
$\tilde{\rho}$	2–10	0.5192	0.0042	$\tilde{\rho}$	7–15	0.5931	0.0041
$f_0/0$	8–16	0.4777	0.0541	$f_0/0$	4–12	0.6553	0.0083
a_1	2–10	0.7184	0.0090	a_1	7–15	0.8126	0.0382
b_1	3–11	0.7073	0.0228	b_1	6–14	0.8615	0.0483
N	7–15	0.7247	0.0285	N	8–16	0.8931	0.0097
N'	7–15	1.135	0.220	N'	8–16	0.9625	0.115

What is immediately clear from these results is that a simple shift in the coupling constant (i.e., in β) is inadequate to reproduce the whole effect of including dynamical quarks as some have suggested. However, a β shift combined with a renormalization of the bare quark mass can bring the spectra into reasonable agreement. We find that the quenched spectrum at $\beta=5.95$ is brought into reasonable agreement with the dynamical quark spectrum at $\beta=5.6$ if we increase the bare masses in the quenched case by a factor of 1.16. The reason we must scale all quark masses by the same factor is because both the quenched and the dynamical Goldstone pions appear to obey PCAC. The new Goldstone pion masses are obtained using PCAC from those at $am_q=0.01$ and $am_q=0.025$. The non-Goldstone pion mass is obtained by noting that the difference between the non-Goldstone and Goldstone pion masses depends only weakly on the mass. ρ and nucleon masses for the "renormalized" masses are obtained from those at $am_q=0.01$ and $am_q=0.025$ by linear interpolation and/or extrapolation. The comparison between these quenched and unquenched masses is exhibited in Tables VII and VIII. These results might have been improved still further if we had varied β in the neighborhood of $\beta=5.95$. The mass differences between the full QCD and quenched masses in Tables VII and VIII are larger than can be attributed to statistics alone, but are probably consistent with the systematic errors due to choices of fits and differences in the finite-size and/or lattice spacing errors between the two theories. It therefore remains to be seen whether there are significant differences in the infinite-volume continuum theories.

IV. CONCLUSIONS

In this work we have extended our earlier work by getting better statistics, not doubling lattices in the time direction and, in the case of $am_q=0.025$, increasing the spatial size. The pion propagator is better behaved than in the previous work on doubled lattices. As always in lattice simulations, the N/ρ mass ratio is too large, although it is decreasing as the quark mass decreases. Similarly, the nucleon-Δ mass splitting is increasing toward its light quark value. In many respects, our systematic errors are larger than the statistical errors. In particular, differences in the nucleon mass obtained from different sources are larger than the apparent errors on each individual mass. Also, estimates of the lattice spacing using different methods give results varying by more than the individual statistical errors. Most of these problems can only be cured by larger scale simulations—larger in the time direction to better isolate asymptotic states, larger physical size in the spatial direction to completely control finite-size effects, smaller quark mass to lessen the need to extrapolate, and smaller physical lattice spacing to approach the continuum limit.

ACKNOWLEDGMENTS

This work was supported by the U.S. Department of Energy under Contracts Nos. DE-FG05-92ER-40742,

TABLE VII. Comparison between quenched hadron spectrum at $\beta=5.95$ and $am_q=0.0116$, and spectrum of full QCD at $\beta=5.6$ and $am_q=0.01$.

Particle	$\beta=5.6$ Mass	$am_q=0.01$ Error	$\beta=5.95$ Mass	$am_q=0.0116$ Error
π	0.2680	0.0010	0.2694	0.0009
$\tilde{\pi}$	0.351	0.004	0.3408	0.0044
ρ	0.518	0.004	0.5244	0.0040
$\tilde{\rho}$	0.515	0.004	0.5271	0.0042
N	0.748	0.004	0.7426	0.0285

TABLE VIII. Comparison between quenched hadron spectrum at $\beta=5.95$ and $am_q=0.029$, and spectrum of full QCD at $\beta=5.6$ and $am_q=0.025$.

Particle	$\beta=5.6$ Mass	$am_q=0.025$ Error	$\beta=5.95$ Mass	$am_q=0.029$ Error
π	0.4189	0.0005	0.4173	0.0008
$\tilde{\pi}$	0.513	0.006	0.4810	0.0020
ρ	0.637	0.005	0.6166	0.0028
$\tilde{\rho}$	0.642	0.004	0.6128	0.0041
N	0.981	0.008	0.9380	0.0097

DE-FG02-85ER-40213, DE-AC02-86ER-40253, DE-AC02-84ER-40125, FG-02-91ER-40661, W-31-109-ENG-38, and by the National Science Foundation under Grants Nos. NSF-PHY87-01775 and NSF-PHY91-16964. The computations were carried out at the Florida State University Supercomputer Computations Research Institute which is partially funded by the U.S. Department of Energy through Contract No. DE-FC05-85ER250000. One of us (D.K.S.) would like to thank S. Kim for familiarizing him with the usage of the CERNLIB minimization routine MINUIT, which was used in obtaining some of the correlated fits, and also to thank him and G. T. Bodwin for many helpful discussions. We thank Jim Hudgens, for his assistance, and T. Kitchens and J. Mandula for their continuing support and encouragement.

[1] For a review of recent progress, see D. Toussaint, in *Lattice '91,* Proceedings of the International Symposium, Tsuhuba, Japan, 1991, edited by M. Fukugita *et al.* [Nucl. Phys. B (Proc. Suppl.) **26**, 3 (1992)]; A. Ukawa, in *Lattice '92,* Proceedings of the International Symposium, Amsterdam, The Netherlands, edited by J. Smit and P. van Baal [Nucl. Phys. B (Proc. Suppl.) **30**, 3 (1993)].

[2] K. Bitar *et al.*, Phys. Rev. Lett. **65**, 2106 (1990); Phys. Rev. D **42**, 3794 (1990).

[3] A. Krasnitz, Phys. Rev. D **42**, 1301 (1990).

[4] K. Bitar *et al.*, in *Lattice '90,* Proceedings of the International Symposium, Tallahassee, Florida, edited by U. M. Heller, A. D. Kennedy, and S. Sanielevici [Nucl. Phys. B (Proc. Suppl.) **20**, 362 (1991)]; in *Lattice '91* [1], p. 259.

[5] K. Bitar *et al.*, in *Lattice '92* [1], p. 3; Phys. Rev. D **48**, 370 (1993).

[6] M. W. Hecht *et al.*, Phys. Rev. D **47**, 285 (1993).

[7] H. C. Andersen, J. Chem. Phys. **72**, 2384 (1980); S. Duane, Nucl. Phys. **B257**, 652 (1985); S. Duane and J. Kogut, Phys. Rev. Lett. **55**, 2774 (1985); S. Gottlieb, W. Liu, D. Toussaint, R. Renken, and R. Sugar, Phys. Rev. D **35**, 2531 (1987).

[8] J. E. Mandula and M. C. Ogilvie, Phys. Lett. B **248**, 156 (1990).

[9] Wall sources were first introduced by the APE Collaboration and are described by E. Marinari, in *Lattice '88,* Proceedings of the International Symposium, Batavia, Illinois, 1988, edited by A. S. Kronfeld and P. B. Mackenzie [Nucl. Phys. B (Proc. Suppl.) **9**, 209 (1989)]. Our particular implementation arose through discussions with G. Kilcup.

[10] C. Liu, in *Lattice '90* [4], p. 149.

[11] A. D. Kennedy, Int. J. Mod. Phys. C **3**, 1 (1992).

[12] R. Gupta, G. Guralnik, G. W. Kilcup, and S. R. Sharpe, Phys. Rev. D **43**, 2003 (1991).

[13] M. F. L. Golterman, Nucl. Phys. **B273**, 663 (1986).

[14] M. F. L. Golterman and J. Smit, Nucl. Phys. **B255**, 328 (1985).

[15] For a discussion of this fitting method, see D. Toussaint, in *From Actions to Answers—Proceedings of the 1989 Theoretical Advanced Summer Institute in Particle Physics,* edited by T. DeGrand and D. Toussaint (World Scientific, Singapore, 1990).

[16] S. Kim and D. K. Sinclair, Phys. Rev. D **48**, 4408 (1993).

[17] R. Altmeyer *et al.*, Nucl. Phys. **B389**, 445 (1993).

[18] P. Bacilieri *et al.*, Phys. Lett. B **214**, 115 (1988).

[19] M. Fukugita, H. Mino, M. Okawa, and A. Ukawa, in *Lattice '90* [4], p. 376; M. Fukugita, N. Ishizuka, H. Mino, M. Okawa, and A. Ukawa, Phys. Rev. D **47**, 4739 (1993).

[20] F. R. Brown *et al.*, Phys. Rev. Lett. **67**, 1062 (1991).

[21] C. Bernard, T. DeGrand, C. Detar, S. Gottlieb, L. Kärkkäinen, R. L. Sugar, and D. Toussaint, Nucl. Phys. B **34**, 366 (1994).

[22] K. M. Bitar *et al.*, Phys. Rev. D **46**, 2169 (1992).

[23] U. M. Heller, K. M. Bitar, R. G. Edwards, and A. D. Kennedy, Report No. FSU-SCRI-94-09 (unpublished).